International Journal of Materials and Chemistry 2014, 4(5): 109-116
DOI: 10.5923/j.ijmc.20140405.02

Preparation and Characterization of Nanocrystalline α-Fe_2O_3 Thin Films Grown by Successive Ionic Layer Adsorption and Reaction Method

M. R. Belkhedkar[1,2], A. U. Ubale[1,*]

[1]Nanostructured Thin Film Materials Laboratory, Department of Physics, Govt. Vidarbha Institute of Science and Humanities, VMV Road, Amravati, Maharashtra, India
[2]Department of Physics, Shri Shivaji College, Akola, Maharashtra, India

Abstract Nanocrystalline α-Fe_2O_3 thin films were deposited by successive ionic layer adsorption and reaction method onto glass substrates. The X-ray diffraction study revealed that α-Fe_2O_3 films are nanocrystalline in nature with rhombohedral structure. The morphological investigations were carried out by using field emission scanning electron and atomic force microscopy studies. The random distribution of α-Fe_2O_3 nano-grains with agglomeration is observed on the substrate surface. The room temperature electrical resistivity of α-Fe_2O_3 film is of the order of $9.46 \times 10^2 \Omega$ cm. The thermo-emf measurements confirmed n-type semiconducting nature of SILAR grown α-Fe_2O_3 films. The optical absorption measurements showed that α-Fe_2O_3 exhibits direct and indirect band gap energies of the order of 1.92 and 2.97eV respectively. These encouraging results make preparation of α-Fe_2O_3 by SILAR method useful in the development of optoelectronic devices such as sensing and photovoltaic devices.

Keywords Thin films, Chemical synthesis, AFM, Optical properties, Electrical properties

1. Introduction

Nanocrystalline transition metal oxide thin films are fascinating materials because their electrical and magnetic properties which have great importance in the field of micro-electronics and nano-electronics, mainly for the development of optoelectronic devices. Materials in nanometer range are found to exhibit new modified physical and chemical properties for wide range of applications. The researchers are extensively investigating simple and economic deposition techniques to grow nanocrystalline metal oxide materials which are suitable substitute for the existing semiconductors. Amongst various metal oxides, iron oxide (α-Fe_2O_3) is a thermodynamically stable oxide of hexagonal close packed crystal structure with indirect and direct band gap energies around 1.9 and 2.7 eV, respectively [1]. In recent years, much attention of scientific community has been focused on iron oxides due to their potential applications such as magnetic devices [2], gas sensor [3-6], humidity sensor [7], solid state lithium ion battery [8], supercapacitor [9], water splitting for hydrogen production [10], solar cell [11, 12], solar filters [13] etc. Apart from this iron oxide nanostructures are technologically important due to their possible applications in many fields including high density magnetic storage devices, magnetic refrigeration systems, catalysis and chemical and biological sensors [14, 15].

In addition to this recently iron oxide has became a novel material for its potential applications in medical science such as drug delivery system, cancer therapy and magnetic resonance imaging due to its biocompatibility, catalytic activity and low toxicity [16–18].

A variety of chemical techniques have been used to fabricate iron oxide thin films such as spray pyrolysis [19, 20], thermal decomposition [21], atomic layer deposition [6], ion-beam assisted deposition [22], electrodeposition [23], RF magnetron sputtering process [24], chemical vapor deposition [25, 26] and SILAR method [27] etc. Among them, SILAR is simple, practical, nonhazardous and low cost soft chemical method. In SILAR technique, nanocrystalline thin films are grown by immersing substrate into separately placed cationic and anionic precursors. In between each immersion substrates are rinsed with purified water, so that only tightly adsorbed layer of species stays on the substrate [28].

In the present work, SILAR method has been developed to grow device quality nanocrystalline iron oxide thin films onto glass substrates as no significant data was published on optical, structural and electrical properties of α-Fe_2O_3 films.

* Corresponding author:
ashokuu@yahoo.com (A. U. Ubale)
Published online at http://journal.sapub.org/ijmc

The prepared iron oxide thin films were characterized using different analytical techniques such as X-ray diffraction (XRD), FTIR spectroscopy, Field Emission Scanning Electron Microscopy (FESEM) and Atomic Force Microscopy (AFM). Optical absorption and electrical resistivity measurements were carried out to find optical band gap and activation energies of α-Fe_2O_3.

2. Experimental

2.1. Deposition of α-Fe_2O_3 Thin Film

Nanocrystalline *α-Fe_2O_3* thin films were deposited by Successive Ionic Layer Adsorption and Reaction method onto glass substrates at room temperature. For the deposition of *α-Fe_2O_3* thin films, 0.05 M ferric chloride of pH 1 was used as a cationic precursor and 0.001M sodium hydroxide of pH *11* was used as an anionic precursor. Before actual deposition glass substrates were boiled in chromic acid, washed with soap solution and finally cleaned with *HCl* and de-ionized water to provide clean substrate surface to achieve uniform deposition. The well cleaned glass substrate was then immersed in a cationic precursor solution for 20s for the adsorption of iron species on the substrate surface. The substrate was then rinsed in de-ionized water for 20s to remove weakly bound species of Fe^{3+} ions from its surface. Once the weakly bound species of Fe^{3+} ions was removed, the substrate was then immersed in an anionic precursor $NaOH$ for 20 s to form a layer of iron oxide material. To remove un-reacted and excess species from substrate, it was rinsed in deionized water for 20 s. This completes one SILAR cycle. By repeating such sixty SILAR cycles, brown coloured, uniform thin films of thickness 251nm were obtained. The films deposited were annealed at 573K for 2h to remove any hydroxide phase formed during the synthesis process and post annealed at 773 *K* temperature for 3h to obtain reddish coloured pure phase of *α-Fe_2O_3*.

2.2. Characterization of α-Fe_2O_3 Thin Film

In the present work, thickness of the film was measured by gravimetric weight difference method using the relation [29],

$$t = \frac{m}{\rho \times A} \quad (1)$$

where m is the mass of the film deposited on the substrate in gram; A is the area of the deposited film in cm^2 and ρ is the density of the deposited material in bulk form (*Fe_2O_3* = 5.242 g/cm^3) [9]. The crystal structure of the film material was identified by X-ray diffraction analysis with D8 Advance, Bruker, Germany diffractometer with monochromatic *CuKα* radiation of wavelength 0.154 nm. The crystallite size of the deposited sample was estimated using the Debye-Scherrer method. The Fourier Transform Infrared (FTIR) spectrum of the sample was collected from Shimadzu make FTIR unit IR Affinity-I. The film morphology was studied by using Field Emission Scanning Electron Microscope (Model: SUPRA 40) and Atomic Force Microscope (Model: Nanonics Multiview 2000^{TM}, Israel). The optical absorption studies were carried out using ELICO ® Double Beam SL 210 UV-VIS Spectrophotometer in the wavelength range 350 to750 nm. Electrical resistivity measurement of sample with temperature was performed using a two-point probe technique with digital electrometer and a stabilized power supply.

3. Results and Discussion

Several deposition trials were performed to optimize concentration of $FeCl_3$ precursor, pH of $NaOH$ solution and number of SILAR deposition cycles. To optimize the concentration of $FeCl_3$ precursor, *α-Fe_2O_3* films were prepared at fix pH of $NaOH$ for 50 SILAR cycles by changing its concentration from 0.03 to 0.3M. Figure 1 shows the variation of *α-Fe_2O_3* film thickness with concentration of $FeCl_3$ precursor. Initially the film thickness rapidly increases from 75 to 192 nm as concentration of $FeCl_3$ increases from 0.03 to 0.05M and above this it decreases slowly. At lower concentration of $FeCl_3$ optimum number of Fe^{3+} ions are available in the solution to form adhesive layer of *α-Fe_2O_3* that gives maximum terminal thickness. But at higher concentration, more Fe^{3+} ions are available in the solution which increases the reaction rate producing rapid precipitate on the substrate surface, which was washed out after rinsing the substrate in water as a result lower terminal thickness is obtained. The optimized concentration of $FeCl_3$ precursor was found to be 0.05M.

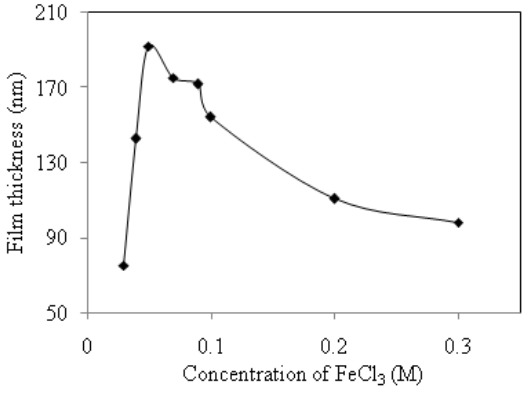

Figure 1. Variation of *α-Fe_2O_3* film thickness with concentration of *$FeCl_3$* solution for 50 SILAR deposition cycles

To optimize pH of $NaOH$ solution, the optimized concentration of $FeCl_3$ (0.05M) and 50 SILAR cycles are kept constant. The variation of *α-Fe_2O_3* film thickness with pH of $NaOH$ is shown in Figure 2. It is observed that at lower pH values ($pH < 8$) the growth rate is very low due to less availability of OH^- ions and it increases up to 11 and it becomes optimum. For $pH > 11$, film thickness decreases due to high growth rate produces less adhesive film which was easily washed out while rinsing in water.

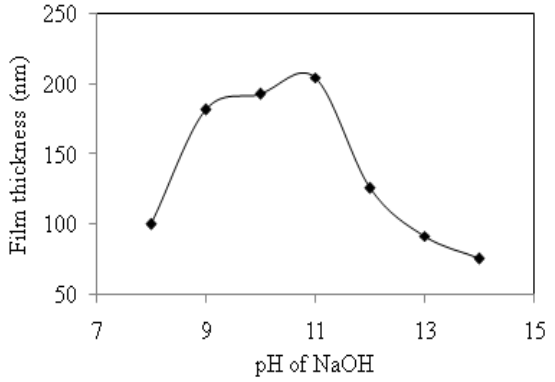

Figure 2. Variation of *α-Fe_2O_3* film thickness with *pH* of *NaOH* solution for 50 SILAR deposition cycles

Figure 3 shows variation of *α-Fe_2O_3* film thickness with number of deposition cycles at the optimized pH and concentration of $FeCl_3$ solution. Initially, film thickness increases up to 60 cycles and then decreases due to peeling of the powdery layer from the substrate surface [30, 31]. Also, by making several trials, the immersion and rinsing time periods were optimized and the values are listed in Table 1.

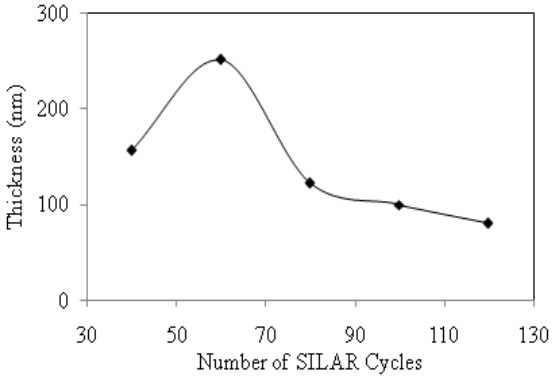

Figure 3. Variation of *α-Fe_2O_3* film thickness with number of SILAR deposition cycles

Table 1. Optimized deposition parameters for the preparation of *α-Fe_2O_3* film

Deposition parameter	Cationic precursor	Anionic precursor
Precursors	*$FeCl_3.4H_2O$*	*NaOH*
Concentrations (M)	0.05	0.001
pH	1	11
Immersion time (s)	20	20
Temperature (K)	303	303
Immersion Cycles	60	60
Volume of precursor (ml)	50	50

3.1. Film Formation Mechanism

Thin films of *α-Fe_2O_3* were prepared by SILAR method onto glass substrates by immersing glass substrates alternately into separately placed cationic and anionic precursors. The deposition mechanism follows the ion-by-ion growth process at nucleation sites on the immersed surfaces. In aqueous solution $FeCl_3$ dissociates as,

$$FeCl_3 \rightarrow Fe^{3+} + 3Cl^- \quad (2)$$

When the glass substrate was immersed in the cationic precursor, Fe^{3+} ions get adsorbed on the substrate due to attractive forces between ions in the solution and that of the surface of the substrate. These forces may be cohesive or vander Waals or chemical attractive [32]. After rinsing in deionized water for 20s, the glass substrate was then immersed in $NaOH$ precursor where Fe^{3+} ions react with OH^- ions to give $Fe(OH)_3$ as,

$$Fe^{3+} + 3OH^- \rightarrow Fe(OH)_3 \quad (3)$$

The $Fe(OH)_3$ deposited on the substrate thermally decomposed to $FeO(OH)$ as,

$$Fe(OH)_3 \xrightarrow{\frac{573K}{2h}} FeO(OH) + H_2O \quad (4)$$

The further annealing of $FeO(OH)$ for 3h at 773K gives *α-Fe_2O_3* [33] as,

$$2FeO(OH) \xrightarrow{\frac{773K}{3h}} Fe_2O_3 + H_2O \quad (5)$$

3.2. Structural Studies

To determine crystal structure and identification of phases of iron oxide thin films synthesized by SILAR method, X-ray diffraction analysis was carried out in the range of angle 2θ between 20 to 80 degree. A typical XRD peak pattern of iron oxide film of thickness 251 nm deposited onto glass substrate is shown in Figure 4. The (0 1 2), (1 0 4), (1 1 6) and (0 1 8) XRD peaks in the pattern confirms rhombohedral *α-Fe_2O_3* (hematite) structure in accordance with JCPDS card 79-0007.

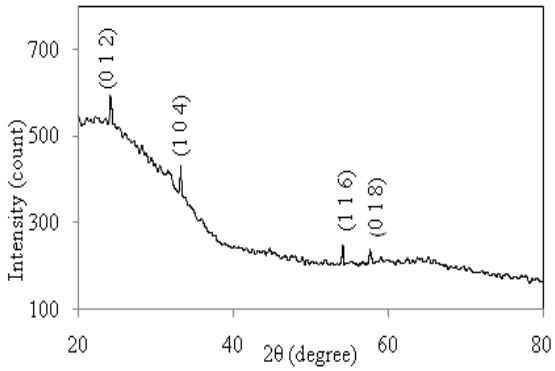

Figure 4. X-ray diffraction pattern of *α-Fe_2O_3* thin film of thickness 251 nm

Comparison of observed XRD data of *α-Fe_2O_3* thin film with the JCPDS card 79-0007 is shown in Table 2. The average crystallite size of the film was determined by using Scherrer formula,

$$D = \frac{0.9\,\lambda}{\beta Cos\,\theta} \quad (6)$$

where λ is the wavelength (0.154 nm); β is the angular line width at half maximum intensity in radians; θ is the Bragg's angle. The average particle size calculated from the prominent peaks (0 1 2) and (1 0 4) is 33 nm.

Table 2. Comparison of observed crystallographic data of *α-Fe_2O_3* thin film with standard JCPDS data card no. 79-0007

h k l	Standard value		Observed value	
	2θ (degree)	d (A^0)	2θ (degree)	d (A^0)
0 1 2	24.180	3.6778	24.167	3.6797
1 0 4	33.198	2.6964	33.186	2.6974
1 1 6	54.137	1.6927	54.140	1.6926
0 1 8	57.664	1.5973	57.682	1.5968

3.3. FTIR Study

For the FTIR measurements, a Shimadzu FTIR spectrometer working in the mid-infrared range from 400 to 4000 cm^{-1} was used. The spectrum was acquired in transmittance mode with a resolution of 1 cm^{-1}. Figure 5 shows FTIR spectra of *α-Fe_2O_3* thin film deposited at temperature 303 K. In the region below 700cm^{-1} two absorption peaks at 617.22 and 455.20 cm^{-1} corresponding to the metal-oxygen (*Fe-O*) vibration modes of the spinel compound are observed. These two Fe-O peaks are sharp and prominent and are in good agreement with literature [9, 34]. The absorption peaks at 717.52 and 952.84 cm^{-1} may be attributed to $Fe-OH$ vibration modes and the peak at 1992.47cm^{-1} is attributed due to $O-H$ stretching [32, 35]. The absorption peaks around 1357.89 and 1492.90 cm^{-1} may be attributed to $O-H$ bending vibrations combined with Fe atoms.

3.4. Surface Morphology

Morphology of the iron oxide thin film deposited onto glass substrate by SILAR method was examined by using FE-SEM image at magnification 44.92 *KX* and 77.93 *KX* (fig.6). The images show random distribution of α-Fe_2O_3 that covers whole substrate surface. Figure 6(A) and 6(B) shows porous granular structures of *α-Fe_2O_3* with agglomeration at some places. The clear separation between the grains in magnified figure indicates vertical growth of *α-Fe_2O_3*. The agglomeration of grains may be due to overgrowth of *α-Fe_2O_3*, as the smaller primary particles have large surface free energy and would tend to agglomerate faster and grow into larger grains. The average grain size of these deposited particles is about 34 nm which is in good agreement with XRD results.

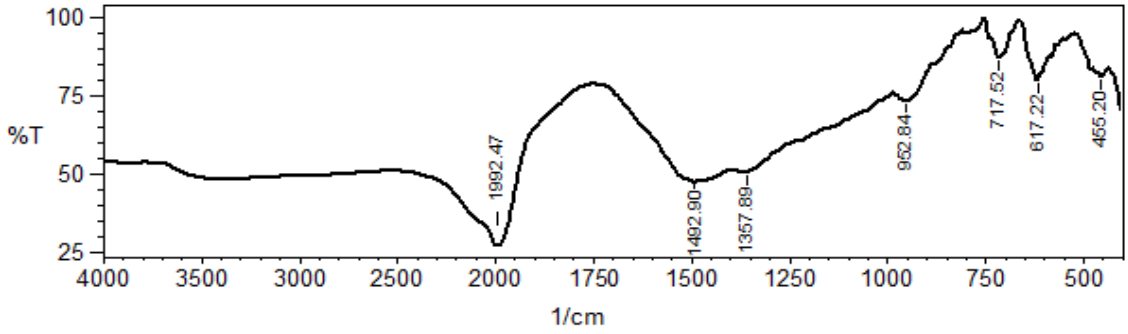

Figure 5. FTIR spectra of the *α-Fe_2O_3* thin film in the range 400-4000cm^{-1}

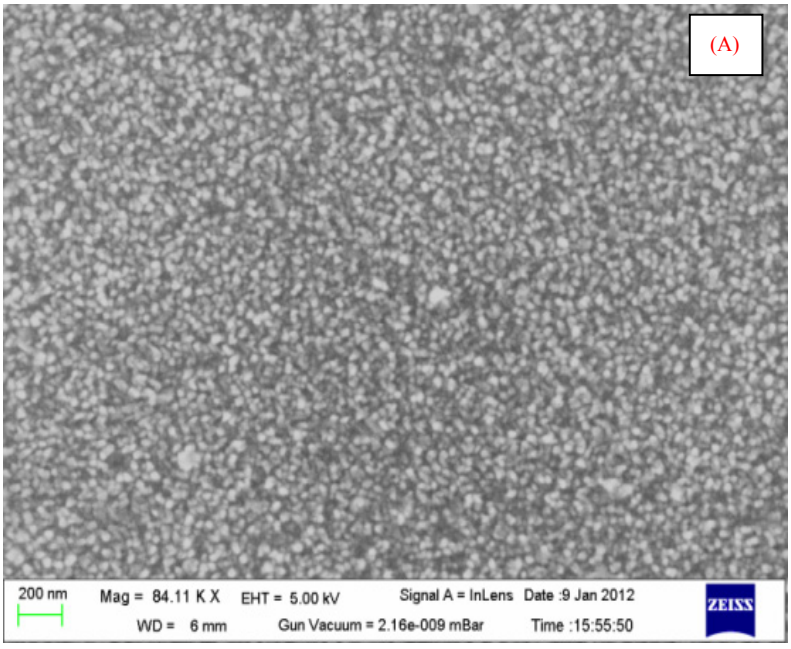

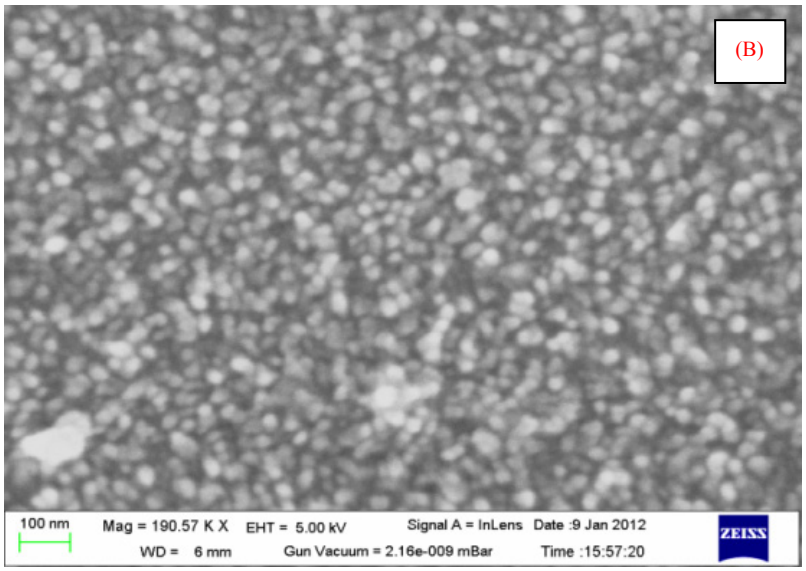

Figure 6. FESEM spectra of α-Fe_2O_3 thin film at magnification: (A) 84.11 KX and (B) 190.57 KX

Elemental analysis of the α-Fe_2O_3 thin film was achieved from the Energy Dispersive X-ray analysis (EDX) spectra presented in Figure 7. The line observed at 6.398 keV is due to K line of Fe element and the line at 0.525 keV is due to K line of oxygen. The additional peaks in the spectra are due to glass substrate especially because of Si and O. The calculated atomic ratio of Fe and O is approximately equal to 2:3 which agrees well with the stoichiometric composition of α-Fe_2O_3.

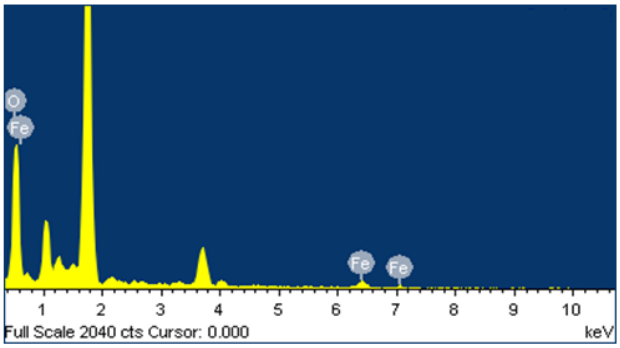

Figure 7. EDAX spectra of α-Fe_2O_3 thin film of thickness 251 nm

The surface morphology of α-Fe_2O_3 film was further analyzed using atomic force microscope having optical fiber tip coated with gold and chromium (Au, Cr) metal with φ = 20 nm at response frequency 52.38 kHz in tapped mode. Figure 8 shows the AFM image of α-Fe_2O_3 film deposited onto glass substrate. The 2D and 3D micrographs are analyzed to understand the roughness, height and grain orientation of α-Fe_2O_3. The 2D micrograph shows rms roughness of the film is 92.32 nm while average roughness is 79.43 nm. The maximum height of the film is 610.02 nm whereas average height is 259 nm which is in agreement with film thickness measured by gravimetric weight difference method. From the 3D micrograph, the grain orientation of α-Fe_2O_3 estimated is found to be 0.07pi.

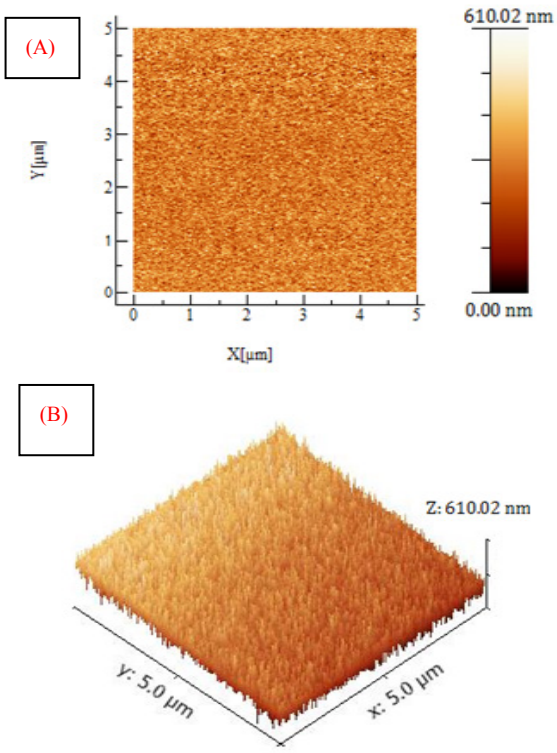

Figure 8. AFM images of α-Fe_2O_3 thin film. (A) 2D image (B) 3D image

3.5. Optical Studies

The optical absorption spectrum of α-Fe_2O_3 thin film was studied in the range of 350-750 nm at room temperature (Figure 9). It appears that α-Fe_2O_3 thin film has high absorbance in the visible region, indicating its applicability as an absorbing material. The optical band gap (Eg) of α-Fe_2O_3 film was calculated using equation [36],

$$\alpha h\upsilon = A(h\upsilon - Eg)^n \quad (7)$$

where, α is absorption coefficient, Eg is optical band gap

energy, A is constant and$n$ is equal to 2 for direct and 1/2 for indirect transition. The plot of $(\alpha h\nu)^{1/2}$ versus $h\nu$ of *α-Fe_2O_3* film is shown in Figure10.

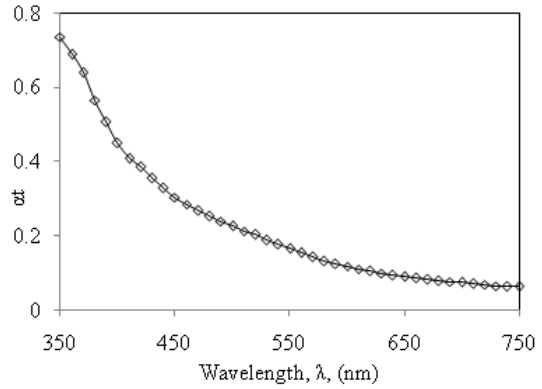

Figure 9. Optical absorption spectra of α-Fe_2O_3 thin films deposited on to glass substrate

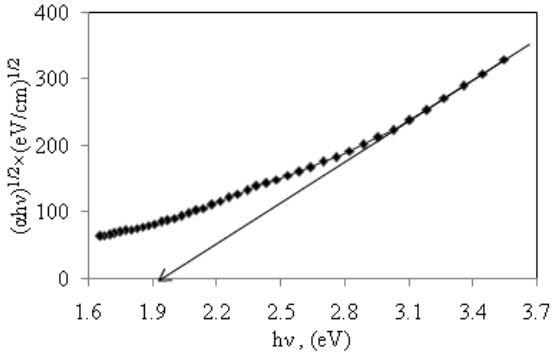

Figure 10. Plot of $(\alpha h\nu)^{1/2}$ versus $h\nu$ of *α-Fe_2O_3* thin film deposited on to glass substrate

From linear nature of the plot, the indirect optical transition in *α-Fe_2O_3* is confirmed. The band gap energy Eg is estimated by extrapolating the linear portion of the plot to the energy axis and is found to be 1.92 eV. Figure 11 shows plot of $(\alpha h\nu)^2$ versus $h\nu$ for *α-Fe_2O_3* film which confirms the presence of direct transition. The optical direct band gap energy of *α-Fe_2O_3* is found to be 2.97 eV. Both the values of band gap energies are quite more than literature which may be due to quantum confinement in the nanocrystalline *α-Fe_2O_3* [1].

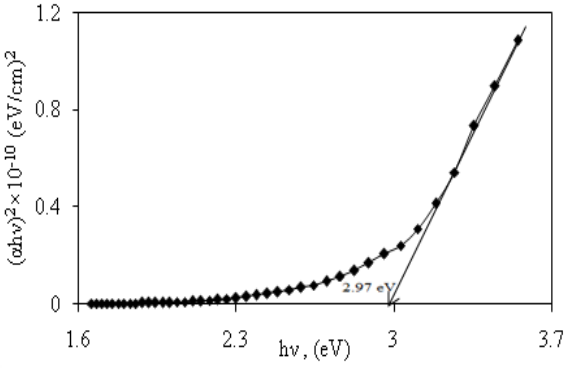

Figure 11. Plot of $(\alpha h\nu)^2$versus $h\nu$ of *α-Fe_2O_3* thin film deposited on to glass substrate

3.6. Electrical Resistivity

The dc two point probe method was employed to understand the variation of electrical resistivity of *α-Fe_2O_3* with temperature. Figure 12 shows the variation of $log(\rho)$ with reciprocal of temperature. It is clearly seen that the resistivity decreases with increase in temperature indicating semiconducting behavior of *α-Fe_2O_3*. The room temperature electrical resistivity of *α-Fe_2O_3* thin film deposited onto glass substrate by SILAR method is of the order of $9.46 \times 10^2 \Omega$ cm, which is very close to reported value ($3 \times 10^2 \Omega$ cm) by A. A. Akl [20] and much less as compared to earlier reports (10^4 Ω cm) [24]. The activation energy was calculated using relation,

$$\rho = \rho_o\left(\frac{E_a}{KT}\right) \quad (8)$$

where, ρ is the resistivity at temperature T, ρ_o is constant, K is Boltzmann constant and E_a is activation energy. The activation energy of *α-Fe_2O_3* thin film deposited onto glass substrate was found 0.1 eV which is in good agreement with the earlier reports [37].

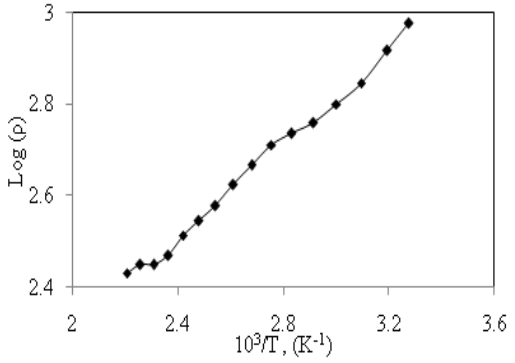

Figure 12. Variation of log of resistivity with reciprocal of temperature of *α-Fe_2O_3* thin film

3.7. Thermoemf Measurement

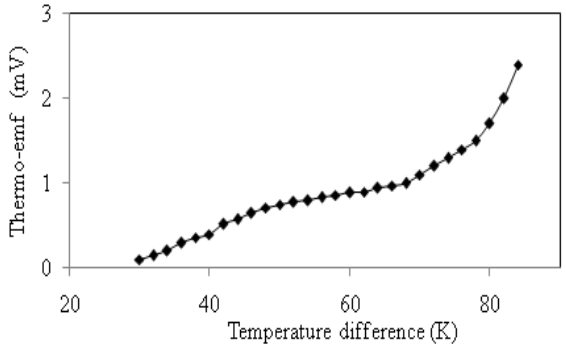

Figure 13. Variation of thermoemf with temperature difference of *α-Fe_2O_3* thin film

To find the type of conductivity of *α-Fe_2O_3*, thermo-emf developed across hot-cold junction was measured as a function of applied temperature dependence (Figure 13). The polarity of thermo-emf was found to be positive towards the hot end with respect to the cold end which confirms that the *α-Fe_2O_3* exhibits n-type semiconducting nature; similar type of conductivity was reported by Balouria et al [38]. The

thermo-emf developed across the film increases with applied temperature difference, which may be because of increased carrier concentration and mobility of charge carriers in the film.

4. Conclusions

In this work, SILAR method has been successfully developed to grow nanostructured iron oxide thin films onto glass substrates. The XRD, FTIR, FESEM, EDX and AFM characterization confirms nanocrystallinity of α-Fe_2O_3. The random distribution of α-Fe_2O_3 nano-grains with agglomeration is observed on the substrate surface. The XRD studies revealed that SILAR grown α-Fe_2O_3 exhibits rhombohedral lattice. The indirect and direct band gap energies are found to be 1.92 and 2.97eV respectively. The porous n-type α-Fe_2O_3 films are semiconducting in nature and have activation energy of the order of 0.1 eV.

REFERENCES

[1] J. A. Glasscock, P. R. F. Barnes, I. C. Plumb, A. Bendavid, P. J. Martin, "Structural, optical and electrical properties of undoped polycrystalline hematite thin films produced using filtered arc deposition", Thin Solid Films, vol.516, pp.1716, 2008.

[2] J. Mallinson, The Foundations of Magnetic Record- ing, second ed., Academic Press, New York, 1993.

[3] S. Wang, W. Wang, W. Wang, Z. Jiao, J. Liu, Y. Qian, "Characterization and gas-sensing properties of nano-crystalline iron_III/oxide films prepared by ultrasonic spray pyrolysis on silicon", Sens. Actuators B vol.69, pp. 22, 2000.

[4] S. Wang, L. Wang et al., "Porous α-Fe_2O_3 hollow microspheres and their application for acetone sensor", J. Solid State Chem., vol. 183, pp. 2869, 2010.

[5] D. Patil, V. Patil, P. Patil, "Highly sensitive and selective LPG sensor based on α-Fe_2O_3 nanorods", Sens. Actu. B, vol. 152, pp. 299, 2011.

[6] M. Aronniemi, J. Saino, J. Lahtinen, "Characterization and gas-sensing behavior of an iron oxide thin film prepared by atomic layer deposition" Thin Solid Films, vol. 516, pp. 6110, 2008.

[7] M. Pelino, C. Colella, C. Cantalini, M. Faccio, G. Ferri, A. D'Amico, "Microstructure and electrical properties of an C–hematite ceramic humidity sensor", Sens. Actuators B, vol.7, pp. 464, 1992.

[8] H. Kitaura, K. Takahashi, F. Mizuno, A. Hayashi, K. Tadanaga, M. Tatsumisago, "Mechanochemical synthesis of α-Fe_{2O3} nanoparticles and their application to all-solid-state lithium batteries", J. Power Sources, vol. 183, pp.418, 2008.

[9] P. M. Kulal, D. P. Dubal, C. D. Lokhande, V. J. Fulari, "Chemical synthesis of Fe_2O_3 thin films for supercapacitor application", J. Alloys Comp., vol. 509, pp. 2567, 2011.

[10] M. Frites, Y. A. Shaban, S. U.M. Khan, "Iron oxide (n-Fe_2O_3) nanowire films and carbon modified (CM)-n-Fe_2O_3 thin films for hydrogen production by photosplitting of water" Int. J. hydrogen energy, vol. 35, vol. 4944, 2010.

[11] J. H. Kennedy, D. J. Dunnwald, "Photooxidation of organic compounds at α-Fe_2O_3 electrodes", Electro-chem. Soc., vol. 130, pp. 2013, 1983.

[12] J. S. Im, S. K. Lee, Y. S. Lee, "Cocktail effect of Fe_2O_3 and TiO_2 semiconductors for a high performance dye-sensitized solar cell", Appl. Surf. Sci., vol. 257, pp. 2164, 2011.

[13] J. C. Galan, R. Almanza, "Solar filters based on iron oxides used as efficient windows for energy savings", Solar Energy, vol. 81, pp. 13, 2007.

[14] V. Sreeja, P. A. Joy," Microwave–hydrothermal synthesis of γ-Fe_2O_3 nanoparticles and their magnetic proper- ties", Mater. Res. Bull., vol. 42, pp. 1570, 2007.

[15] J. Du, H. Liu, "Preparation of super paramagnetic γ-Fe_2O_3 nanoparticles in nonaqueous medium by γ -irradiation" J. Magn. Magn. Mater., vol. 302, pp. 263, 2006.

[16] X. Jing, Y. Haibin, F. Wuyou, D. Kai, Y. Sui, J. Chen, Y. Zeng, M. Li, G. Zou, J. Magn. Magn. Mater., vol. 309, pp. 307, 2007.

[17] B. Fang, G. Wang, W. Zhang, M. Li, X. Kan, "Fabrication of Fe_3O_4 nanoparticles modified electrode and its application for voltammetric sensing of dopamine", Electroanalysis, vol. 17, pp.744, 2005.

[18] A. K. Gupta, M. Gupta, "Synthesis and surface engineering of iron oxide nanoparticles for biomedical applications", Biomater., vol. 26, pp. 3995, 2005.

[19] R. N. Goyal, D. Kaur, A. K. Pandey, "Growth and characterization of iron oxide nanocrystalline thin films via low-cost ultrasonic spray pyrolysis", Mater. Chem. Phys., vol.116, pp. 638, 2009.

[20] A. A. Akl, "Microstructure and electrical properties of iron oxide thin films deposited by spray pyrolysis" Appl. Surf. Sci., vol. 221, pp. 319, 2004.

[21] J. Hua, Y. Heqing, "Thermal decomposition synthesis of 3D urchin-like α-Fe_2O_3 superstructures", Mater. Sci. Engg. B., vol. 156, pp. 68, 2009.

[22] Y. J. Park, K. M. A. Sobahan, C. K. Hwangbo, "Optical and structural properties of Fe_2O_3 thin films prepared by ion-beam assisted deposition", Surf. Coat. Technol., vol. 203, pp. 2646, 2009.

[23] S. S. Kulkarni, C. D. Lokhande, "Structural, optical, electrical and dielectrical properties of electrosynth-sized nanocrystalline iron oxide thin films", Mater. Chem. Phys., vol.82, pp. 151, 2003.

[24] J. D. Uribe, J. Osorio, C. A. Barrero, D. Girata, A. L. Morales, A. Hoffmann, "Physical properties in thin films of iron oxides", J. Microelectro., vol. 39, pp.1391, 2008.

[25] H. G. Cha, C. W. Kim, Y. H. Kim, M. H. Jung, E. S. Ji, B. K. Das, J. C. Kim, Y. S. Kang, "Preparation and characterization of α-Fe_2O_3 nanorod-thin film by metal–organic chemical vapor deposition", Thin Solid Films, vol. 517, pp. 1853, 2009.

[26] K. Shalini, G. N. Subbanna, S. Chandrasekaran, S. A.

Shivashankar, "Thin films of iron oxide by low presure MOCVD using a novel precursor: tris (*t*-butyl-3-oxo-butanoato) iron (III)", Thin Solid Films, vol.424, pp. 56, 2003.

[27] S. Park, "Preparation of iron oxides using ammonium iron citrate precursor: Thin films and nanoparticles", J. Solid State Chem., vol. 182, pp. 2456, 2009.

[28] A. U. Ubale, M. R. Belkhedkar, Y. S. Sakhare, A. Singh, C. Gurada, D.C. Kothari, "Characterization of nanostructured Mn_3O_4 thin films grown by SILAR method at room temperature", Mater. Chem. Phys., vol. 136, pp. 1067, 2012.

[29] M. R. Belkhedkar, A.U. Ubale, Physical properties of nanostructured Mn_3O_4 thin films synthesized by SILAR method at room temperature for antibacterial application, J. Mol. Struct., vol. 1068, pp. 94, 2014.

[30] A. U. Ubale, A. N. Bargal, "Characterization of nano structured photosensitive (*NiS*) *x* (*CdS*) (*1-x*) composite thin films grown by successive ionic layer adsorption and reaction (SILAR) route", Mater. Res. Bull., vol. 46, pp. 1000, 2011.

[31] A. U. Ubale, D. K. Kulkarni, "Studies of size dependent properties of cadmium telluride thin films deposited by Successive Ionic Layer Adsorption and Reaction (SILAR) method", Ind. Pure. Appl. Phy., vol. 44, pp. 254, 2006.

[32] H. M. Pathan, C. D. Lokhande, "Deposition of metal chalcogenide thin films by successive ionic layer adsorption and reaction (SILAR) method" Bull. Mater. Sci., vol. 27, pp.85, 2004.

[33] W. Y. Hsien, Z. L. Dong, C. F. Li, S. K. Yen, "Characterization of electrolytic deposited *α-Fe_2O_3* thin films on stainless steel as anodes for Li-ion batteries", Surf. Coat. Tech., vol. 216, pp. 52, 2013.

[34] S. Zhan, D. Chen, X. Jiao, S. Liu, "Facile fabrication of long *α-Fe_2O_3*, *α-Fe* and *γ-Fe_2O_3* hollow fibers using solgel combined co-electrospinning technology", J. Coll. Interf. Sci., vol. 308, pp. 265, 2007.

[35] J. Sharma, S. K. Tripathi, 'Effect of deposition pressure on structural, optical and electrical properties of zinc selenide thin films", Physica B, vol. 406, pp. 1757, 2011.

[36] A. U. Ubale, Y. S. Sakhare, M. V. Bhute, M. R. Belkhedkar, A. Singh, "Size dependent structural, electrical and optical properties of nanostructured iron selenide thin films deposited by Chemical Bath Deposition Method", Solid State Sci., vol.16, pp. 134, 2013.

[37] A. Boudjemaa, S. Boumaza, M. Trari, R. Bouarab, A. Bouguelia," Physical and photoelectrochemical characterizations of *α-Fe_2O_3*. Application for hydrogen production", Int. J. hydrogen energy, vol. 34, pp. 4268, 2009.

[38] V. Balouria, A. Kumar, S. Samanta, A. Singh, A. K. Debnath, A. Mahajan, R. K. Bedi, D. K. Aswal, S. K. Gupta," Nano-crystalline *Fe_2O_3* thin films for ppm level detection of H_2S", Sens. Actu. B, vol. 181, pp. 471, 2013.